Mechanism and Machine Theory 173 (2022) 104850

Contents lists available at ScienceDirect

Mechanism and Machine Theory

journal homepage: www.elsevier.com/locate/mechmt

Research paper

The kinematic design of redundant robots for maximizing failure-tolerant workspace size

Ashraf M. Bader *, Anthony A. Maciejewski

Department of Electrical and Computer Engineering, Colorado State University, Fort Collins, Colorado 80523-1373, USA

ARTICLE INFO

Keywords:
Kinematically redundant robots
Locked-joint failure
Failure-tolerant workspace
Failure-tolerant robot design

ABSTRACT

It has been shown that one can guarantee a reachable workspace for a kinematically redundant robot after an arbitrary locked-joint failure if one artificially restricts the range of its joints prior to the failure. This work presents an algorithm for computing the optimal kinematic parameters and artificial joint limits for a robot to maximize this so-called "failure-tolerant workspace". The proposed technique employs a genetic algorithm that incorporates a novel method for selecting an initial population that results in fast convergence to high-quality solutions. The algorithm is illustrated on multiple examples of kinematically redundant robots and is shown to be computationally tractable even for robots that perform tasks in 6D workspaces.

1. Introduction

Kinematically redundant robots can complete a specific task even after a joint failure has occurred, due to the extra degrees of freedom (DOF) that are in addition to the minimum required to perform a specified task. This advantage is important for robots that are employed in applications where performing routine maintenance and/or repair is not possible, for example, in hazardous and remote environments. Example applications include nuclear reactors [1,2], space exploration [3], and deep-sea exploration [4]. Previous studies have used fault trees to assess a robot's reliability [5,6] and other work has been focused on implementing tolerance to failures including fault diagnosis [7], detection [8], and identification [9,10]. The locked-joint failure is the most common model used for these previous studies. This is because a joint is locked due to the failure itself or because fail-safe brakes are employed, e.g., to deal with free-swinging joint failures where the torque of the actuator is lost [11].

The various techniques used for designing failure-tolerant robots can be characterized based on whether they use local or global measures of how much a robot's dexterity is affected by a failure. The local measures are frequently quantified by the singular values of the Jacobian matrix at a specific robot configuration. Optimizing these values have been used in both the design and control of failure-tolerant robots [12–15]. The global measures are those that are not configuration dependent, e.g., the total reachable workspace of a robot. In previous work, the failure-tolerant workspace ($\mathcal{W}_F$) has been defined as the guaranteed reachable workspace both before and after an arbitrary locked-joint failure [16,17].

One way to guarantee the existence of $\mathcal{W}_F$ is by increasing the degree of redundancy (DOR) by two for each potential joint failure. This high degree of redundancy is required because of the worst-case scenario where a joint failure is at a configuration that eliminates two degrees of freedom [18]. Later studies have shown that one can guarantee the existence of $\mathcal{W}_F$ for a robot with only one DOR by restricting the joints limits prior to a failure, i.e., so-called "artificial joint limits" that are software joint limits imposed to restrict joint motion to be within specified range [19]. These artificial limits are imposed to prevent the robot from failing in a worst-case configuration and are released after the occurrence of an arbitrary locked-joint failure.

* Corresponding author.
E-mail addresses: Ashraf.Bader@ColoState.edu (A.M. Bader), Anthony.Maciejewski@ColoState.edu (A.A. Maciejewski).

https://doi.org/10.1016/j.mechmachtheory.2022.104850
Received 1 December 2021; Received in revised form 10 February 2022; Accepted 19 March 2022
Available online 6 April 2022

A number of optimization techniques have been discussed to maximize $\mathcal{W}_F$ for planar workspaces. A brute force technique has been used to determine artificial joint limits that are constrained to be symmetrical around zero for planar 3R and 4R robots [20]. Another study has presented a gradient ascent method to compute the optimal link lengths and artificial joint limits that maximize $\mathcal{W}_F$ by computing the symbolic expressions for the area of $\mathcal{W}_F$ and its gradient [21]. In 6D workspaces (3D position and 3D orientation), the coordinate ascent method has been used to optimize only the artificial joint limits for a particular robot, i.e., the kinematic parameters of the robot are constant [22]. Therefore, the solution space is bounded by 2π for each of the artificial joint limits and so the size of $\mathcal{W}_F$ is periodic with a period of 2π.

None of the above optimization techniques for maximizing $\mathcal{W}_F$ are applicable for determining the optimal kinematic parameters for robots that are to perform 6D tasks. This is due to the dramatically higher number of variables, that both increases the computational cost and the likelihood of convergence to local maxima. In this work, a technique based on Genetic Algorithms (GA) is proposed to design optimally fault-tolerant kinematically redundant robots, i.e, an optimal set of kinematic parameters and artificial joint limits, for any number of degrees of freedom and workspace dimensions. The advantages of using a GA-based approach is that it is more likely to converge to a globally optimal solution and, if appropriately implemented, to converge faster when parallelism is exploited. However, to achieve these advantages one must develop a method to appropriately select the pool of initial candidate solutions.

The remaining sections are presented in the following manner. The required background on computing the failure-tolerant workspace is reviewed in the next section. In Section 3, we first formally define the optimization problem. We then present our GA-based technique for determining an optimal solution, including our novel approach for generating an effective initial population. We illustrate the procedure using a 4 DOF spatial positioning robot. The effectiveness of our technique is shown in Section 4, where we provide three kinematic designs for robots that are optimally fault tolerant. These designs, as well as the optimal artificial joint limits, are given for tasks in a variety of workspaces including the fully general 6D spatial case. Finally, the conclusions are in Section 5.

2. Background on computing failure-tolerant workspace[1]

2.1. Overview

The definition of the failure-tolerant workspace, $\mathcal{W}_F$, as previously discussed in [17,21,22], is summarized in this section. In those works, artificial limits were applied on the joints before a failure, which were then released after a failure of one of the joints was identified. Applying artificial limits will typically decrease the pre-failure workspace, however, if chosen appropriately, they guarantee a post-failure workspace. As in previous work, we assume that the robot is kinematically redundant, i.e., $n > m$ where n is the number of the joints, m is the workspace dimension, DOR $= n - m$, and the physical limits of joint i are from -2π to 2π.

2.2. Definition of failure-tolerant workspace

The forward kinematic function, denoted $\mathbf{f}$, maps the joint space, $\mathcal{C} \subset \mathbb{R}^n$, to the workspace, denoted $\mathcal{W} \subset \mathbb{R}^m$. Let the n-dimensional vector θ represent the joint angles in the joint space, i.e., $\theta \in \mathcal{C}$, and the m-dimensional vector $\mathbf{x}$ represent the robot's end-effector position and/or orientation in the workspace, i.e., $\mathbf{x} \in \mathcal{W}$. Therefore, the forward kinematic equation is given by

$$\mathbf{x} = \mathbf{f}(\theta). \tag{1}$$

Prior to failure, the lower $\underline{a}_i$ and upper $\overline{a}_i$ artificial joint limits are the joint i restrictions where $\underline{a}_i$ and $\overline{a}_i \in [-2\pi,\ 2\pi]$, and $i = \{1, 2, \ldots, n\}$. The pre-failure configuration space, denoted $\mathcal{C}_A$, is the joint space before joint failure, i.e., $\mathcal{C}_A = A_1 \times \cdots \times A_n$ where $A_i = [\underline{a}_i,\ \overline{a}_i]$ is the range of joint angles between $\underline{a}_i$ and $\overline{a}_i$. The pre-failure workspace, denoted $\mathcal{W}_0$, is the reachable workspace obtained by mapping $\mathcal{C}_A$ into the workspace,

$$\mathcal{W}_0 = \mathbf{f}(\mathcal{C}_A) = \{\mathbf{x} = \mathbf{f}(\theta) \mid \theta \in \mathcal{C}_A\}. \tag{2}$$

After joint i fails and is locked at $\theta_i = q_i$ where $\underline{a}_i \le q_i \le \overline{a}_i$, the artificial limits are released on the remaining working joints. This results in the reduced configuration space that is a hyperplane at $\theta_i = q_i$ in the configuration space $\mathcal{C}$,

$${}^i\mathcal{C}(q_i) = \{\theta \in \mathcal{C} \mid \theta_i = q_i\}. \tag{3}$$

The guaranteed reachable workspace after joint i fails at q_i between $\underline{a}_i \le q_i \le \overline{a}_i$ is the post-failure workspace, denoted $\mathcal{W}_i$, and is given by

$$\mathcal{W}_i = \bigcap_{\underline{a}_i \le q_i \le \overline{a}_i} \mathbf{f}({}^i\mathcal{C}(q_i)). \tag{4}$$

The guaranteed reachable workspace both before and after an arbitrary single locked-joint failure is the failure-tolerant workspace,

$$\mathcal{W}_F = \bigcap_{i \in \mathbf{F} \cup \{0\}} \mathcal{W}_i, \tag{5}$$

where $\mathbf{F} \subset \{1, 2, \ldots, n\}$ is the failure index for the joints that are prone to failures.

[1] Section II is very similar to those in [21,22], and is included here to provide the background to make this paper self-contained.

2.3. Identification of the failure-tolerant workspace

Previous work [17] has identified two conditions for determining if a workspace location $\mathbf{x}$ belongs to $\mathcal{W}_F$. The pre-image of $\mathbf{x}$, denoted $\mathbf{f}^{-1}(\mathbf{x})$, that is given by

$$\mathbf{f}^{-1}(\mathbf{x}) = \{\boldsymbol{\theta} \in \boldsymbol{C} \mid \mathbf{f}(\boldsymbol{\theta}) = \mathbf{x}\} \tag{6}$$

is used to formulate both conditions. Condition 1 is that $\mathbf{x}$ be reachable prior to a failure, i.e., $\mathbf{x} \in \mathcal{W}_\mathbf{0}$, so that

$$\boldsymbol{C}_A \cap \mathbf{f}^{-1}(\mathbf{x}) \neq \emptyset. \tag{7}$$

The above condition states that there must be an intersection between the pre-failure configuration space, $\boldsymbol{C}_A$, and the pre-image of $\mathbf{x}$, $\mathbf{f}^{-1}(\mathbf{x})$, for at least one configuration. Condition 2 is that $\mathbf{x}$ is reachable after a failure, i.e., $\mathbf{x} \in \mathcal{W}_i$ for $i \in \mathbf{F}$, so that

$$A_i \subset P_i[\mathbf{f}^{-1}(\mathbf{x})] \tag{8}$$

where P_i is the projection onto the ith joint axis, i.e., the range of θ_i for all $\boldsymbol{\theta}$ that satisfy $\mathbf{x} = \mathbf{f}(\boldsymbol{\theta})$. Condition 2 means that after joint i is locked at $\theta_i = q_i$ where $\underline{a}_i \leq q_i \leq \overline{a}_i$, the workspace point $\mathbf{x}$ can still be reached because q_i is contained in the ith component of $\mathbf{f}^{-1}(\mathbf{x})$. If both conditions are satisfied for $\mathbf{x}$, then $\mathbf{x} \in \mathcal{W}_F$.

Fortunately, it is relatively straightforward to identify all potential boundaries of $\mathcal{W}_F$. The potential boundaries of $\mathcal{W}_\mathbf{0}$ are located at $\mathbf{f}(\boldsymbol{\theta})$ where the configuration $\boldsymbol{\theta} \in \boldsymbol{C}_A$ is a kinematic singularity or when one or more joints are at an artificial joint limit, i.e., $\theta_i = \underline{a}_i$ or $\theta_i = \overline{a}_i$. The potential boundaries of $\mathcal{W}_i$ are the workspace locations where the end effector is on the verge of violating condition 2. This can occur in two ways, i.e., either the projection of the pre-image for this workspace location becomes disjoint within A_i or it fails to contain an endpoint of A_i. The first way will occur at $\mathbf{f}(\boldsymbol{\theta})$ where $\boldsymbol{\theta} \in {}^i\boldsymbol{C}\ (q_i)$ is a kinematic singularity. The second situation can be identified by computing the null vector associated with the robot's Jacobian. In particular, let $\mathbf{n}(\boldsymbol{\theta})$ represent the null vector of the robot at configuration $\boldsymbol{\theta}$ and $\mathbf{n}_i$ be the ith element of $\mathbf{n}$. Then the potential boundaries of $\mathcal{W}_i$ occur when $n_i = 0$ and $\theta_i = \underline{a}_i$ or $\overline{a}_i$. Once all potential boundaries of $\mathcal{W}_\mathbf{0}$ and all $\mathcal{W}_i$'s are determined, one can use the two conditions to identify the boundaries of $\mathcal{W}_F$ [17].

2.4. Estimation of failure-tolerant workspace size

Using the two conditions from the previous section, one can use the technique that is described in [22] to estimate the volume of the failure-tolerant workspace. Assume that joint 1, i.e., the base joint, is a revolute joint.[2] The pre-image of a workspace point $\mathbf{x}$, i.e., the set of configurations that correspond to $\mathbf{x}$, is given by (6). If one rotates $\mathbf{x}$ about the rotation axis of joint 1 by $\beta \in [-\pi,\ \pi]$, then the pre-image of the rotated $\mathbf{x}$, denoted $\mathbf{x}'$, is computed by evaluating (6) for $\mathbf{x}'$ where $\mathbf{x}' = \boldsymbol{R}_z\mathbf{x}$, and

$$\boldsymbol{R}_z = \begin{bmatrix} \cos(\beta) & -\sin(\beta) & 0 \\ \sin(\beta) & \cos(\beta) & 0 \\ 0 & 0 & 1 \end{bmatrix}. \tag{9}$$

The pre-image of $\mathbf{x}'$ is identical to that of $\mathbf{x}$ except that every configuration's joint one value is related by $\theta_1' = \theta_1 + \beta$. This simple relationship means that one does not have to compute the pre-images for the entire workspace, i.e., one of the dimensions can be easily inferred.

The general approach for estimating the volume of a 3D spatial workspace is to first discretize a half plane into square grids, where the normal of the half-plane is perpendicular to the rotation axis of joint 1. One then needs to compute a 3D volume element by determining the rotation angle range, denoted $[\underline{\beta}_F, \overline{\beta}_F]$, of a grid center, denoted $\mathbf{c}_g$, about the rotational axis of joint 1. The rotation angle range of $\mathbf{c}_g$ is defined as the range where the rotated $\mathbf{c}_g$ belongs to $\mathcal{W}_F$, i.e., when the pre-image of the rotated $\mathbf{c}_g$ satisfies conditions 1 and 2 from Section 2.3.

Thus, the integration of the grid area over its rotation angle range is the failure-tolerant 3D volume element,

$$v_F \approx \int_{\underline{\beta}_F}^{\overline{\beta}_F} r\ \Delta g\ d\beta_F, \tag{10}$$

where r is the shortest distance from the grid center, $\mathbf{c}_g$, to the axis of joint 1, and Δg is the grid area.

It is important to note that the pre-image of a grid center may consist of a union of disjoint self-motion manifolds (SMM). The ranges of $[\underline{\beta}_F,\ \overline{\beta}_F]$ for these disjoint SMMs may, or may not, overlap. If two ranges overlap, then they are replaced with the union of those two ranges, until no overlapping ranges remain. Let $\mathbf{B}$ denote the set of non-overlapping ranges of $[\underline{\beta}_F,\ \overline{\beta}_F]$ for a given grid center. Therefore, to compute the volume associated with a grid center one must compute (10) for each range in $\mathbf{B}$. Thus, the summation of all the volumes for all grids is the failure-tolerant workspace volume, denoted $\mathcal{V}_F$, i.e.,

$$\mathcal{V}_F \approx \sum_{i=1}^{N_{c_g}} \sum_{j=1}^{|\mathbf{B}|} v_F(i,j), \tag{11}$$

[2] If the first joint is prismatic, an analogous procedure can be performed.

where N_{c_g} is the number of reachable grid centers.

For a 6D hypervolume element, one can apply the Monte-Carlo integration technique described in [14,23] using uniform random sampling of orientations at a workspace point to estimate the failure-tolerant orientation volume, denoted $\mathcal{V}_{F_o}$,

$$\mathcal{V}_{F_o} \approx \frac{N_F}{N_o}\pi^2 \tag{12}$$

where N_F is the number of failure-tolerant orientations, N_o is total number of randomly selected orientations, and π^2 is the maximum orientation volume. Then, by adding (12) to the integrand of (10), a 6D hypervolume element is given by

$$v_F \approx \int_{\underline{\beta}_F}^{\overline{\beta}_F} (r\ \Delta g)\left(\frac{N_F}{N_o}\pi^2\right) d\beta_F. \tag{13}$$

where the rotation angle range, $[\underline{\beta}_F, \overline{\beta}_F]$, is determined by the range where N_F is constant. The entire 6D hypervolume of the failure-tolerant workspace is estimated by computing (11) using (13).

One can also use (11) to estimate the volume or hypervolume of the original workspace, denoted $\mathcal{W}_{\mathbf{0}_{\max}}$, which is the robot's workspace with no restrictions applied on the robot's joints. For tasks defined as position-only, Eq. (10) is evaluated with integration limits of $-\pi$ to π. If the task is defined by position and orientation, then (13) is evaluated with integration limits of $-\pi$ to π and N_F is replaced by the number of reachable orientations, denoted $N_{o_{\max}}$.

Let the unit of measure for the failure-tolerant workspace size be denoted S_F and the original workspace size be denoted $S_{0_{\max}}$. This general measure may represent any combination of linear and rotational components, e.g., the failure-tolerant workspace size for planar robots that perform a task defined as a 2D position or 2D position with orientation, or for spatial robots that perform tasks that are 3D position or 3D position with 3D orientation. In cases where S_F and $S_{0_{\max}}$ are combinations of different units, e.g., meters and radians for position and orientation, a suitable normalization factor should be employed to make sure that S_F and $S_{0_{\max}}$ are meaningful measures.

3. Method

3.1. Definition of the problem

The goal of this work is to determine the kinematic design and artificial joint limits for a redundant robot that maximizes the size of its failure-tolerant workspace. The kinematic design of an n DOF robot can be defined by the Denavit and Hartenberg (DH) parameters for each joint i, i.e., the link twist, α_i, the link length, l_i, the joint offset, d_i, and the joint angle, θ_i. In this work, we limit the range of these parameters to the following values: $-\pi/2 \le \alpha_i \le \pi/2$, $0 \le l_i \le 1$, $-1 \ge d_i \ge 1$, $-2\pi \le \theta_i \le 2\pi$.

In addition to the kinematic parameters, one needs to determine the set of artificial joint limits, denoted $\boldsymbol{A}$, that consists of the lower and upper limits of joint i, i.e., $\boldsymbol{A} = \{\underline{a}_1, \overline{a}_1, \underline{a}_2, \overline{a}_2, \dots, \underline{a}_n, \overline{a}_n\}$, where $\underline{a}_i \le \theta_i \le \overline{a}_i$. Because S_F is rotationally invariant to θ_1, only the size of the interval $A_1 = [\underline{a}_1, \overline{a}_1]$ is relevant. Therefore, the constraint that $\underline{a}_1 = -\overline{a}_1$ is imposed to reduce the number of variables in the optimization.

To provide a fair comparison between the kinematic designs for robots of vastly different sizes, one would normalize S_F by the workspace size of the robot without any joint limits, i.e., $S_{0_{\max}}$. Therefore, the optimization problem for maximizing the failure-tolerant workspace size can be formulated as:

$$\underset{l_i, d_i, \alpha_i, \boldsymbol{A}}{\text{maximize}} \quad \frac{S_F}{S_{0_{\max}}}. \tag{14}$$

For cases when a specific robot is given, i.e., the DH parameters are constant, the optimization problem (14) can be solved for $\boldsymbol{A}$ as the only decision variable.

3.2. Genetic algorithm

3.2.1. Overview

In this section we describe a genetic algorithm that is used to solve the optimization problem given in (14). Genetic algorithms are a global optimization technique where chromosomes are used to encode the decision variables and the operations of crossover and mutation are used to iteratively search the entire solution space. Each iteration creates a new population of chromosomes and is referred to as a generation. The stochastic selection of chromosomes for crossover is used to improve the likelihood that new generations will include better solutions. The preservation of the fittest chromosomes from the previous generation, referred to as elitism, guarantees that solution quality is monotonically increasing. The convergence of GAs will typically be improved by seeding the initial population with chromosomes that have high fitness values.

In this section we illustrate the implementation of our specific GA using a simple 4 DOF robot that is designed to perform 3D spatial positioning tasks. Each chromosome consists of the decision variables, where each gene represents one of the kinematic parameters or artificial joint limits. For spatial robots the number of decision variables is $5n-1$, so that for our illustrative example there are nineteen variables. The eight kinematic parameters of l_is and d_is where $i = \{1, 2, 3, 4\}$ are given in meters. The remaining eleven variables, i.e., the α_is and the artificial joint limits are given in degrees. The size of the population for a GA is frequently proportional to the number of decision variables, e.g., $\times$ 20, so that for the 4 DOF robot the population size has been chosen to be 380.

3.2.2. Initial population

The first step in executing a GA is to determine an initial population. Frequently, chromosomes are generated at random, however, it is likely that random chromosomes will have very low (or zero) fitness values. Therefore, it is common to "seed" the initial population with chromosomes that are selected by an appropriately chosen heuristic to have relatively high fitness values. To determine these seed chromosomes for the optimization problem described by (14) one can first randomly select the genes that correspond to feasible kinematic parameters and then compute the genes that represent good artificial joint limits for the resulting robot using a heuristic.

In the 4 DOF spatial robot case, the selection of kinematic parameters must result in a robot that is physically able to perform a task in a 3D positioning workspace. Therefore, the rotation axes of the four joints must not be nearly parallel and the values of the l_is and d_is must not be too small so that the robot has a reasonably sized workspace. After the kinematic parameters of the robot are selected, the artificial joint limits, $\boldsymbol{A}$, for that robot can be selected so that they satisfy (8) for at least some points in the workspace as follows.

One should first randomly select a reachable workspace point that is not close to a workspace boundary and then guarantee that it satisfies both conditions for being in $\mathcal{W}_F$ by appropriately selecting the artificial joint limits. This can be done by computing the critical points on a self-motion manifold (SMM), i.e., a manifold consisting of all joint values that correspond to the robot's end effector being at the selected workspace point. The artificial joint limits, $\underline{a}_i$ and $\overline{a}_i$, are then set to the values of these critical points, which are the minimum and maximum values of θ_i over the entire SMM. Frequently, a workspace point will have multiple disjoint SMMs so one should select the one that gives the largest ranges for $\boldsymbol{A}$. In addition, by avoiding points near a workspace boundary, this approach avoids SMMs that are very small in size. The proposed technique for computing $\underline{a}_i$s and $\overline{a}_i$s guarantees that the selected chromosomes will have non-zero fitness values, i.e., $\frac{S_F}{S_{0_{\max}}} > 0$. Fig. 1(a) shows the improvement in the fitness values of selected chromosomes by comparing the histograms of chromosomes that are selected randomly to those selected with the proposed heuristic. In that figure, 87% of the randomly selected chromosomes resulted in a zero fitness value, with the maximum fitness value being less than 2.6%. In addition to resulting in no chromosomes with zero fitness, the proposed heuristic results in fitness values up to $\frac{S_F}{S_{0_{\max}}} \approx 9\%$. In practice, roughly 75% of the initial population should be selected using the proposed heuristic with the remaining 25% selected at random. This ratio was determined from initial studies on low-dimensional robots and is done to prevent premature convergence to locally optimal solutions. After the initial population is generated, one can compute the next new generation of chromosomes as presented in the following section.

3.2.3. Generating a new population

The new generation of chromosomes are potential optimal chromosomes of decision variables, i.e., the kinematic parameters and artificial joint limits. A new generation is computed from the current generation in the following manner. First, the top 5% of the fittest chromosomes in the current generation are included in the next generation in order to implement elitism. Then, the remaining 95% are generated by selecting two parents using stochastic selection and applying two-point crossover to generate two children, both of which are included in the new population. Next, 15% of these children are selected for possible mutation. Each gene of these children has a 0.01 probability of being mutated. If selected for mutation, the value of this gene is replaced with a random value from the range of the variable as defined in Section 3.1. The values of the parameters used here come from initial studies on low-dimensional robots.

3.2.4. Case study of a 4 DOF spatial positioning robot

We illustrate the proposed GA by computing the kinematic parameters and artificial joint limits for a simple 4 DOF spatial positioning robot that maximizes $S_F/S_{0_{\max}}$. The technique described in Section 2.4 is used to estimate the fitness function. Eq. (11) is used to compute both S_F and $S_{0_{\max}}$ using a grid side length that is 4% of the maximum reach of the robot. This maximum reach is different for each chromosome because of the different kinematic parameters.

We first illustrate the importance of seeding the initial population with chromosomes that have nonzero fitness values. Fig. 1(b) shows the different rates of convergence between a completely random initial population and those that are seeded with selected chromosomes. The evolution of the GA using a random initial population is shown in red, illustrating a much lower starting fitness value and converging to a lower final fitness value when compared to the seeded initial population shown in blue. This holds true for all examples shown later in Section 4. For the 4 DOF case, seeded populations converged to a final solution after 100 generations whereas random populations required twice as many generations. After convergence, one can run a local optimization technique, such as coordinate ascent [22], to improve the final design.

The results from the optimization shown in Fig. 1, i.e., the DH parameters and $\boldsymbol{A}$, are given in Table 1 and illustrated in Fig. 2. The robot is shown in two different configurations, i.e., stretched out in (a) and with its joints at the middle of the artificial joint limits in (b). The resulting fault-tolerant workspace $\mathcal{W}_F$ is shown in (c) along with the robots original workspace $\mathcal{W}_{\mathbf{0_{max}}}$ in (d). The optimization criterion, i.e., the ratio of the size of these two workspaces $S_F/S_{0_{\max}}$, is equal to 19.2%. To provide some context, one can compare the $S_F/S_{0_{\max}}$ value of this optimized robot to that of traditional designs. For example, it is not uncommon for robots to have an $S_F/S_{0_{\max}} = 0$. In particular, this is true for anthropomorphic robot designs because $S_F = 0$ due to the elbow joint being failure intolerant [24]. Even robot designs optimized for local fault-tolerance, do not have large values for $S_F/S_{0_{\max}}$. For example, when one computes the optimal $\boldsymbol{A}$ for the previously designed 4 DOF spatial positioning robot in [25], $S_F/S_{0_{\max}}$ is less than 2%. In the next section, we show how increasing the DOR from 1 to 2 affects the size of the failure-tolerant workspace and how the proposed GA technique is computationally tractable for designing 7 DOF robots that perform tasks in six-dimensional workspaces.

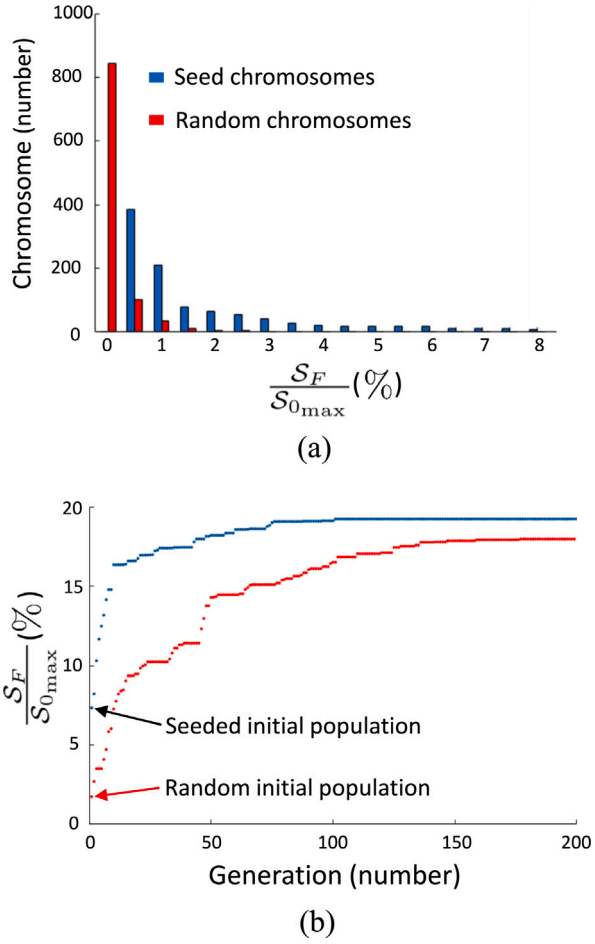

Fig. 1. This figure illustrates the effectiveness of using seeded chromosomes over random chromosomes for the case of a 4 DOF spatial robot, i.e., robots with DOR = 1. In (a) the histogram of 1000 randomly generated chromosomes is compared to 1000 selected chromosomes generated by the proposed technique. Approximately 87% of the random chromosomes (shown in red) have an $S_F/S_{0_{\max}} = 0$ whereas all of the seeded chromosomes (shown in blue) are non-zero and reach fitness values of nearly 9%. The impact of these selected chromosomes on the evolution of the GA is shown in (b), where for each generation the highest fitness value is plotted. Both the final maximum fitness value and the rate of convergence are improved. The final corresponding robot design and its resulting workspace are shown in Fig. 2 with the values of the DH parameters and $\boldsymbol{A}$ given in Table 1. (For interpretation of the references to color in this figure legend, the reader is referred to the web version of this article.)

Table 1
Optimal DH parameters and $\boldsymbol{A}$ for a 4 DOF spatial positioning robot.

$Link_i$	α_i [degrees]	l_i [meters]	d_i [meters]	θ_i [degrees]	
				$\underline{a}_i$	$\overline{a}_i$
1	85°	0.50	−0.29	−146°	146°
2	−53°	0.48	0	−234°	10°
3	−89°	0.76	0.05	−115°	132°
4	68°	0.95	1	−101°	118°

4. Examples

4.1. Overview

In this section we use the proposed technique to design redundant robots that maximize the failure-tolerant workspace sizes. We determine these robots for three illustrative examples as follows. The first example considers how increasing the DOR affects the $\mathcal{W}_F$ for planar robots that operate in a 3D workspace, i.e., 2D position and 1D orientation. We present two planar robots that have been designed with 4 DOF and 5 DOF, i.e., DORs of 1 and 2. We then illustrate how increasing the DOR for the 4 DOF spatial

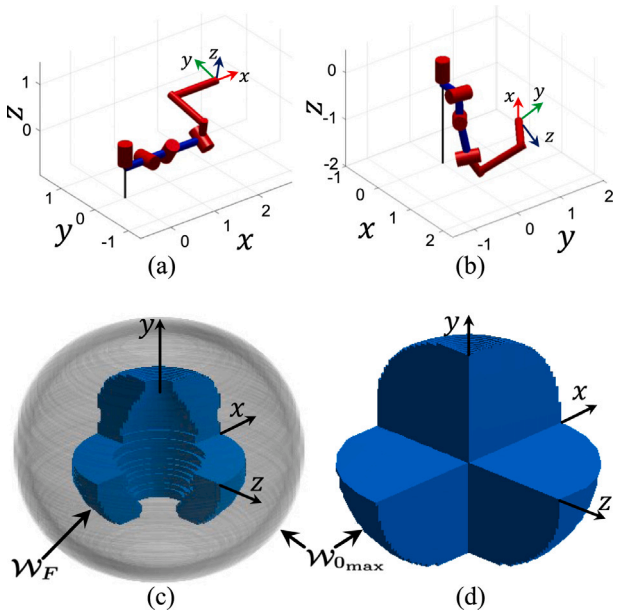

Fig. 2. This figure shows the robot design and the corresponding workspaces that resulted from the GA optimization shown in Fig. 1. All position units used in the subfigures are measured in meters. An isometric view of the designed robot where it is stretched out is shown in (a), and in a configuration where all the joints are at the middle of their optimal artificial joint limits is shown in (b). The DH parameters and $\boldsymbol{A}$ for this 4 DOF spatial positioning robot are given in Table 1. Shown in (c) is $\mathcal{W}_F$ using orthogonal cross sections to show more of the internal structure, where the volume is $\mathcal{S}_F = 18.69$ m^3. For comparison, the boundary of $\mathcal{W}_{\mathbf{0}_{\max}}$ is overlayed in gray. All of $\mathcal{W}_{\mathbf{0}_{\max}}$ is shown in (d), again using orthogonal cross sections, where $\mathcal{S}_{0_{\max}} = 97.38$ m^3. The optimal value of $\mathcal{S}_F/\mathcal{S}_{0_{\max}} = 19.2\%$.

positioning robot described in the previous section affects its $\mathcal{W}_F$ that is shown in Fig. 2. Lastly, we present the optimal design for a 7 DOF spatial robot that performs tasks in a 6D spatial workspace (3D position and 3D orientation).

In all examples, the technique described in Section 2.4 is used to estimate the workspace sizes, $\mathcal{S}_F$ and $\mathcal{S}_{0_{\max}}$. We use the same sampling resolution of the workspace that was used in previous work [22]. For the planar robots, we set Δg to be equal to 4% of the robot's maximum reach, which results in 25 line segments over the length of the arm. We also select 25 orientation samples, i.e., $N_o = 25$, for the 1D orientation in the 3D planar case. In the 3D and 6D spatial workspaces, Δg is the area of a square grid where the length of a grid side is selected to be 4% of the robot's maximum reach. We use $N_o = 200$ to sample the 3D orientations in the 6D workspace.

4.2. Planar positioning and orienting robot designs

Previous work [22] has determined the optimal artificial joint limits for equal link length planar robots. Here, we determine the optimal kinematic parameters, i.e, the link lengths, denoted $\boldsymbol{L} = \{l_1, l_2, \ldots, l_n\}$, as well as the artificial joint limits, to illustrate how much the size of the failure tolerant workspace can be improved. In order to have a fair comparison, we constrain the total length of the arm to be the same as in the equal link length case.

For the 4 DOF planar robot case, the GA converged to a design where $\mathcal{S}_F/\mathcal{S}_{0_{\max}} = 10.5\%$ as shown in Fig. 3. The size of the failure-tolerant workspace increased by 57% as compared to the previous equal link length result in [22]. Fig. 3 also shows that some locations in the workspace have a reachable failure-tolerant orientation of 70% as compared to a maximum of 47% in the equal link length example in [22].

When we increased the DOR to 2, i.e., 5 DOF planar robots, the GA converged to a design where $\mathcal{S}_F/\mathcal{S}_{0_{\max}}$ reached 46% as shown in Fig. 4. In comparison, the equal link length case in [22] has an $\mathcal{S}_F/\mathcal{S}_{0_{\max}}$ value of 31%. It is interesting to note that an increase in the DOR from 1 to 2 has dramatically increased the value of $\mathcal{S}_F/\mathcal{S}_{0_{\max}}$ from 10.5% to 46% in the design of planar robots.

4.3. Spatial robot designs

We now look at how increasing the DOR of the 4 DOF spatial positioning robot designed in Section 3 (Table 1 and Fig. 2) affects the failure tolerant workspace. Applying the GA for a 5 DOF spatial robot design, i.e., a robot with DOR of 2, resulted in the robot given in Table 2 and shown in Fig. 5. This robot has an $\mathcal{S}_F/\mathcal{S}_{0_{\max}}$ of 79% which is a dramatic increase over the 19.2% of the 4 DOF robot. It is interesting to note that joints 1 and 2 are identical for the optimal 5 DOF robot, albeit with different artificial joint limits.

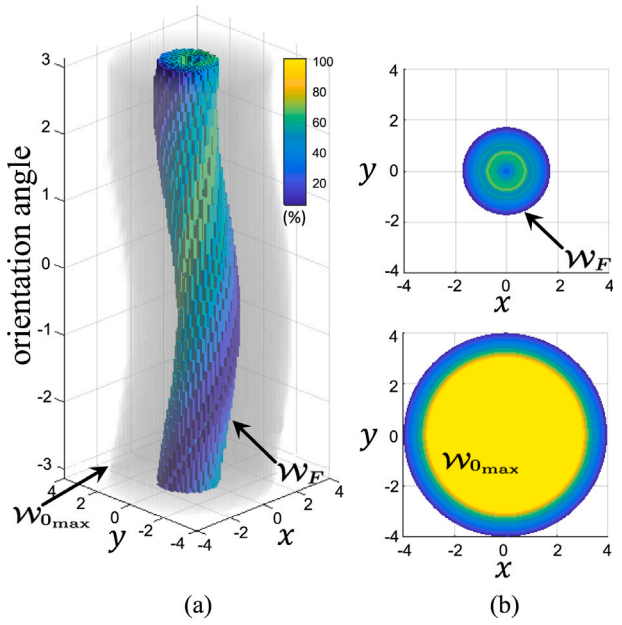

Fig. 3. This figure shows the 3D planar workspace (2D position and 1D orientation) of an optimal 4 DOF planar robot design. All position units used in the subfigures are measured in meters and the orientation angle in radians. The color at a workspace position indicates the percentage of orientations that are achievable at that position. The 3D view in (a) shows the 2D position workspace and the orthogonal third axis is the orientation angle where $\mathcal{W}_F$ is shown in solid colors and the gray boundary is the outer boundary of $\mathcal{W}_{0_{max}}$. In (b) the top view of $\mathcal{W}_F$ and $\mathcal{W}_{0_{max}}$ are shown. The maximum value of $S_F/S_{0_{max}} = 10.5\%$ where $S_F = 26$ m^2 rad and $S_{0_{max}} = 245$ m^2 rad. The optimal robot's kinematic parameters are $\boldsymbol{L} = [1.14, 1.24, 1.14, 0.48]$ and $\boldsymbol{\Lambda} = \{-180°, 180°, 90°, 143°, 90°, 143° -180°, 180°\}$.

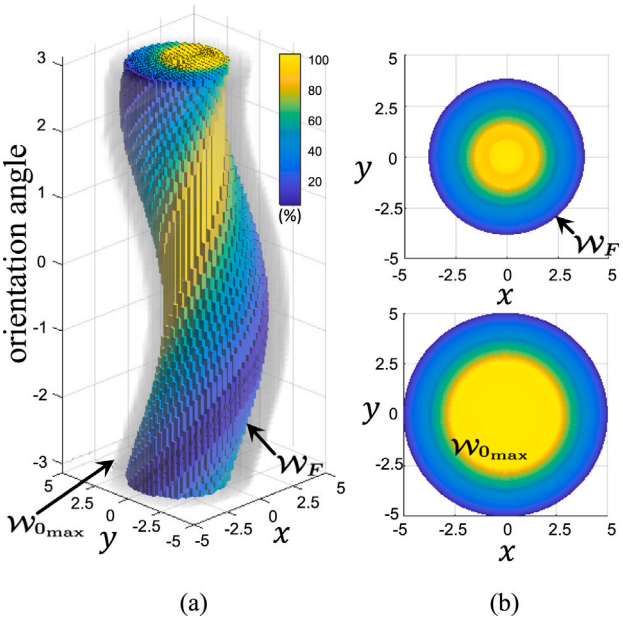

Fig. 4. This figure shows the 3D planar workspace (2D position and 1D orientation) of an optimal 5 DOF planar robot design. All position units used in the subfigures are measured in meters and the orientation angle in radians. The color at a workspace position indicates the percentage of orientations that are achievable at that position. The 3D view in (a) shows the 2D position workspace and the orthogonal third axis is the orientation angle where $\mathcal{W}_F$ is shown in solid colors and the gray boundary is the outer boundary of $\mathcal{W}_{0_{max}}$. In (b) the top view of $\mathcal{W}_F$ and $\mathcal{W}_{0_{max}}$ are shown. The maximum value of $S_F/S_{0_{max}} = 46\%$ where $S_F = 67$ m^2 rad and $S_{0_{max}} = 145$ m^2 rad. The optimal robot's kinematic parameters are $\boldsymbol{L} = [0.4, 0.77, 1, 0.4, 0.77]$ and $\boldsymbol{\Lambda} = \{-180°, 180°, -180°, 180°, 110°, 115°, -180°, 180°, -180°, 180°\}$.

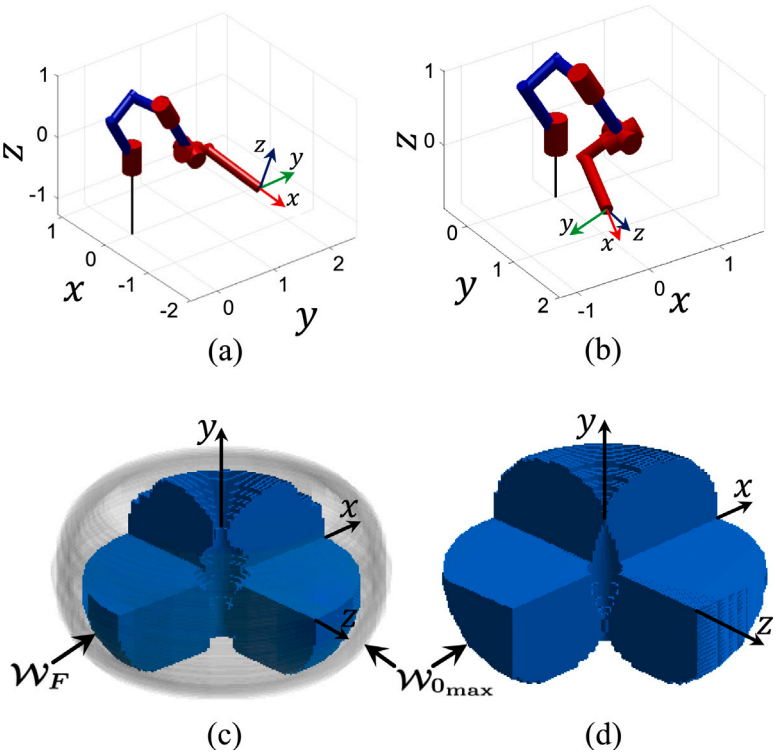

Fig. 5. This figure shows the optimal 5 DOF robot designed for 3D positioning along with the corresponding workspaces. All position units used in the subfigures are measured in meters. An isometric view of the designed robot where it is stretched out is shown in (a), and in a configuration where all the joints are at the middle of their optimal artificial joint limits is shown in (b). The DH parameters and $\boldsymbol{A}$ for this 5 DOF spatial positioning robot are given in Table 2. Shown in (c) is $\mathcal{W}_F$ using orthogonal cross sections to show more of the internal structure, where the volume is $S_F = 16$ m^3. For comparison, the boundary of $\mathcal{W}_{0_{max}}$ is overlayed in gray. All of $\mathcal{W}_{0_{max}}$ is shown in (d), again using orthogonal cross sections, where $S_{0_{max}} = 20.2$ m^3. The optimal value of $S_F/S_{0_{max}} = 79\%$.

Table 2
Optimal DH parameters and $\boldsymbol{A}$ for a 5 DOF spatial positioning robot.

$Link_i$	α_i [degrees]	l_i [meters]	d_i [meters]	θ_i [degrees]	
				$\underline{a}_i$	$\bar{a}_i$
1	0°	0	0	−42°	42°
2	30°	0.65	1	20°	297°
3	90°	0	−1	−80°	225°
4	70°	0	0	140°	293°
5	−80°	1	−0.5	0°	180°

4.4. Spatial positioning and orienting robot designs

In our final example we illustrate that the proposed GA technique is computationally tractable for designing 7 DOF robots that perform tasks in six-dimensional (positioning and orienting) workspaces. The optimal solution for the DH parameters and $\boldsymbol{A}$ are given in Table 3 and the resulting robot design, along with its workspaces, are shown in Fig. 6. The size of the failure-tolerant workspace is 109 m^3 rad^3 out of a prefailure maximum workspace of 1217 m^3 rad^3, i.e., $S_F/S_{0_{max}} = 9\%$.

Table 4 shows the optimal normalized failure-tolerant workspace sizes, $S_F/S_{0_{max}}$, that result from optimal robot designs, i.e., optimal kinematic parameters and artificial joint limits. Cases 1–3 are for positioning workspaces where cases 4–6 are for positioning and orientating workspaces. It should be noted that, in general, comparing cases 1–3 with 4–6 for the same DOR, the normalized S_F for positioning and orienting workspaces are much smaller than for purely positioning workspaces. Consider case 1 to be the base line case where the optimal 3R planar positioning robot has 1 DOR. If one increases the task space of case 1 by 1-dimension in positioning, as in case 2, then $S_F/S_{0_{max}}$, is reduced to 19.2%, however, if it is increased by adding orientation, as in case 4, then it is reduced significantly more to 10.5%. One can also see this same trend by comparing cases 3 and 5. Both cases have the same m and DOR but case 3, which has a purely positioning workspace, has a $S_F/S_{0_{max}} = 79\%$ whereas case 5, which includes orientation in its workspace, only has an$S_F/S_{0_{max}} = 46\%$.

Another trend is that the value of $S_F/S_{0_{max}}$ decreases as one increases the dimension of the task space, m, if the DOR is held constant. This is clear by comparing cases 1, 2, 4, and 6, each with DOR= 1. This is not surprising because one DOR is being

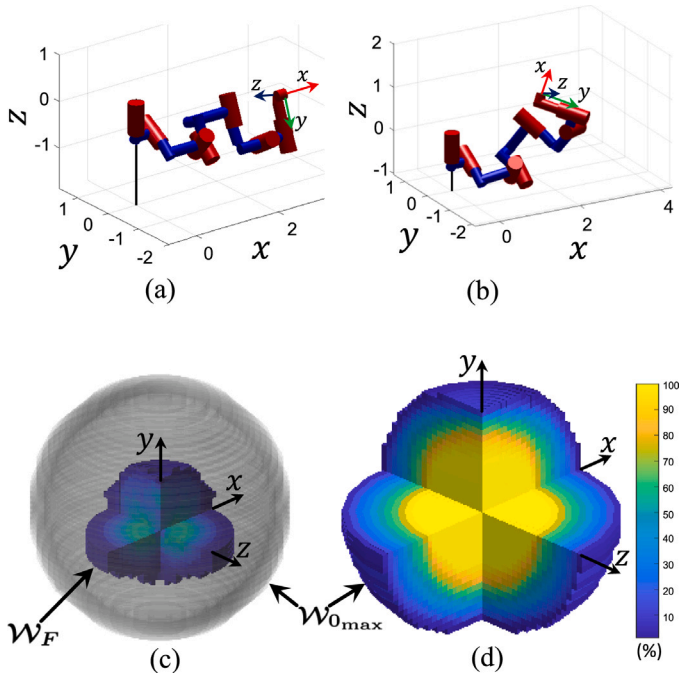

Fig. 6. This figure shows the optimal 7 DOF robot designed for 6D positioning and orienting along with the corresponding workspaces. All position units used in the subfigures are measured in meters. An isometric view of the designed robot where it is stretched out is shown in (a), and in a configuration where all the joints are at the middle of their optimal artificial joint limits is shown in (b). The DH parameters and $\boldsymbol{A}$ for this 7 DOF positioning and orienting robot are given in Table 3. Shown in (c) is $\mathcal{W}_F$ using orthogonal cross sections to show more of the internal structure, where the volume is $S_F = 109$ m^3 rad^3. The color at a workspace position indicates the percentage of orientations that are achievable at that position. For comparison, the boundary of $\mathcal{W}_{\mathbf{0}_{\max}}$ is overlayed in gray. All of $\mathcal{W}_{\mathbf{0}_{\max}}$ is shown in (d), again using orthogonal cross sections, where $S_{0_{\max}} = 1217$ m^3 rad^3. The optimal value of $S_F/S_{0_{\max}} = 9\%$.

Table 3
Optimal DH parameters and $\boldsymbol{A}$ for a 7 DOF spatial positioning and orienting robot.

$Link_i$	α_i [degrees]	l_i [meters]	d_i [meters]	θ_i [degrees]	
				$\underline{a}_i$	$\overline{a}_i$
1	−62°	0.4	−0.4	−107°	107°
2	−79°	0.8	−0.6	−164°	141°
3	90°	0.2	0.2	−132°	132°
4	29°	1	0.6	−151°	102°
5	81°	0.6	−0.8	−115°	149°
6	−80°	0.4	0.2	−75°	129°
7	−90°	0.2	0.8	16°	193°

Table 4
Size of optimal normalized failure-tolerant workspaces.

Case number	Workspace dimension [m]		DOF [n]	DOR [$m-n$]	$S_F/S_{0_{\max}}$
	Position	Orientation			
1	2D	–	3	1	33.3%[a]
2	3D	–	4	1	19.2%
3	3D	–	5	2	79%
4	2D	1D	4	1	10.5%
5	2D	1D	5	2	46%
6	3D	3D	7	1	9%

[a]Case 1 is the optimal normalized S_F of a 3R planar positioning robot from [21].

distributed over a larger number of DOF. (If the DOR is held constant then the DOF increases as m is increased.) However, the amount of decrease in $S_F/S_{0_{\max}}$ becomes smaller as m increases, e.g., the drop from case 4 to case 6 is smaller than the drop from case 1 to either case 2 or 4. Finally, it is important to note that increasing the DOR for the same m will dramatically increase the size of the normalized failure-tolerant workspace. This increase is more than a factor of four when comparing case 2 with 3 and case 4 with 5.

5. Conclusion

This work presented a technique to determine the kinematic design of a redundant robot that maximizes the size of its failure-tolerant workspace. The proposed technique is based on a genetic algorithm that optimizes both the Denavit and Hartenberg parameters and artificial joint limits. The GA uses an efficient hybrid approach to estimate the sizes of workspaces. The efficient performance of the GA relies on a novel technique for identifying a good initial population, which results in faster convergence and higher quality final solutions. This proposed technique is applicable to the design of any arbitrary redundant robot, regardless of the number of degrees of freedom, and is computationally tractable even for robots that perform tasks in 6D workspaces. This is significant because other techniques, i.e., gradient ascent and coordinate ascent optimization techniques [21,22], become infeasible for higher degrees of freedom. It is shown that even a single degree of redundancy can guarantee a significant failure tolerant workspaces size. Furthermore, the addition of a second degree of redundancy dramatically increases the failure-tolerant workspace size by up to a factor of four. Finally, it is shown that the size of failure-tolerant workspaces where end-effector orientation control is required are relatively smaller than for purely positioning tasks.

Declaration of competing interest

The authors declare that they have no known competing financial interests or personal relationships that could have appeared to influence the work reported in this paper.

References

[1] J. Petereit, J. Beyerer, T. Asfour, S. Gentes, B. Hein, U.D. Hanebeck, F. Kirchner, R. Dillmann, H.H. Götting, M. Weiser, M. Gustmann, T. Egloffstein, ROBDEKON: Robotic systems for decontamination in Hazardous environments, in: Proc. IEEE Int. Symp. Safe, 2019, pp. 249–255.
[2] R. Guzman, R. Navarro, J. Ferre, M. Moreno, Rescuer: Development of a modular chemical, biological, radiological, and nuclear robot for intervention, sampling, and situation awareness, J. Field Robot. 33 (7) (2016) 931–945.
[3] Z. Mu, L. Han, W. Xu, B. Li, B. Liang, Kinematic analysis and fault-tolerant trajectory planning of space manipulator under a single joint failure, Robot. Biomim. 3 (1) (2016) 16.
[4] S. Soylu, B.J. Buckham, R.P. Podhorodeski, Redundancy resolution for underwater mobile manipulators, Ocean Eng. 37 (2–3) (2010) 325–343.
[5] B. Harpel, J.B. Dugan, I.D. Walker, J.R. Cavallaro, Analysis of robots for hazardous environments, in: Proc. IEEE Annu. Rel. Maintainability Symp., 1997, pp. 111–116.
[6] T.A. Ferguson, L. Lu, Fault tree analysis for an inspection robot in a nuclear power plant, IOP Conf. Ser. Mater. Sci. Eng. 235 (1) (2017) 012003.
[7] F. Xu, Z. Yang, J. Hu, G. Jiang, G. Dai, Fault diagnosis of a selective compliance assembly robot arm manipulator based on the end joint motion analysis: Threshold algorithm and experiments, Trans. Inst. Meas. Control 40 (5) (2018) 1691–1700.
[8] A.S. Rezazadeh, H.R. Koofigar, S. Hosseinnia, Adaptive fault detection and isolation for a class of robot manipulators with time-varying perturbation, J. Mech. Sci. Technol. 29 (11) (2015) 4901–4911.
[9] M.L. McIntyre, W.E. Dixon, D.M. Dawson, I.D. Walker, Fault identification for robot manipulators, IEEE Trans. Robot. 21 (5) (2005) 1028–1034.
[10] H. Chang, P. Huang, M. Wang, Z. Lu, Locked-joint failure identification for free-floating space robots, in: IEEE Int. Conf. Inf. Autom., 2014, pp. 170–175.
[11] C. Gang, G. Wen, J. Qingxuan, W. Xuan, F. Yingzhuo, Failure treatment strategy and fault-tolerant path planning of a space manipulator with free-swinging joint failure, Chin. J. Aeronaut. 31 (12) (2018) 2290–2305.
[12] F.L. Hammond III, Synthesis of kth order fault-tolerant kinematically redundant manipulator designs using relative kinematic isotropy, Int. J. Adapt. Innov. Syst. 2 (1) (2014) 73–96.
[13] C.S. Ukidve, J.E. McInroy, F. Jafari, Using redundancy to optimize manipulability of Stewart platforms, IEEE/ASME Trans. Mechatronics 13 (4) (2008) 475–479.
[14] K.M. Ben-Gharbia, A.A. Maciejewski, R.G. Roberts, Kinematic design of manipulators with seven revolute joints optimized for fault tolerance, IEEE Trans. Syst. Man Cybern. 46 (10) (2016) 1364–1373.
[15] Y. She, W. Xu, H. Su, B. Liang, H. Shi, Fault-tolerant analysis and control of SSRMS-type manipulators with single-joint failure, Acta Astronaut. 120 (2016) 270–286.
[16] C.J.J. Paredis, W.K.F. Au, P.K. Khosla, Kinematic design of fault tolerant manipulators, Comput. Electr. Eng. 20 (3) (1994) 211–220.
[17] R.C. Hoover, R.G. Roberts, A.A. Maciejewski, P.S. Naik, K.M. Ben-Gharbia, Designing a failure-tolerant workspace for kinematically redundant robots, IEEE Trans. Autom. Sci. Eng. 12 (4) (2015) 1421–1432.
[18] C.J.J. Paredis, P.K. Khosla, Designing fault-tolerant manipulators: How many degrees of freedom? Int. J. Robot. Res. 15 (6) (1996) 611–628.
[19] C.L. Lewis, A.A. Maciejewski, Fault tolerant operation of kinematically redundant manipulators for locked joint failures, IEEE Trans. Robot. Autom. 13 (4) (1997) 622–629.
[20] R.S. Jamisola, Optimization of failure-tolerant workspaces for redundant manipulators, Philipp. Sci. Lett. 3 (2010) 66–75.
[21] A.M. Bader, A.A. Maciejewski, Maximizing the failure-tolerant workspace area for planar redundant robots, Mech. Mach. Theory 143 (2020) 103635.
[22] A.M. Bader, A.A. Maciejewski, A hybrid approach for estimating the failure-tolerant workspace size of kinematically redundant robots, IEEE Robot. Autom. Lett. 6 (2) (2020) 303–310.
[23] C. Chen, D. Jackson, Parameterization and evaluation of robotic orientation workspace: A geometric treatment, IEEE Trans. Robot. 27 (4) (2011) 656–663.
[24] K.M. Ben-Gharbia, A.A. Maciejewski, R.G. Roberts, Modifying the kinematic structure of an anthropomorphic arm to improve fault tolerance, in: IEEE Int. Conf. Robot. Automat., 2015, pp. 1455–1460.
[25] K.M. Ben-Gharbia, A.A. Maciejewski, R.G. Roberts, Kinematic design of redundant robotic manipulators for spatial positioning that are optimally fault tolerant, IEEE Trans. Robot. 29 (5) (2013) 1300–1307.